Quantitative and Qualitative Evaluation for Gamma Radiographic Image Enhancement

H. Kasban[1], O. Zahran[2], H. Arafa[1], M. El-Kordy[2], S. M. S. Elaraby[1] and F. E. Abd El-Samie[2]

[1]Engineering Department, Nuclear Research Center, Atomic Energy Authority, Egypt
E-mails: Hany_kasban@yahoo.com, selaraby@netscape.net
[2]Department of Electronics and Electrical Communications, Faculty of Electronic Engineering, Menofia University, Menouf, 32952, Egypt.
E-mails: osama_zahran@menofia.edu.eg, dr_elkordy08@yahoo.com, fathi_sayed@yahoo.com

Abstract

This paper presents some image processing techniques that can be used for radiographic image enhancement. Contrast enhancement, filtering, denoising, and interpolation processes are carried out in this paper. Contrast enhancement is carried out using adaptive histogram equalization. Filtering is carried out using median, Wiener, Lee, and Kuan filters. Wavelet and curvelet transforms are used for image denoising. Three interpolation are carried out. The results are evaluated qualitatively and quantitatively using the Peak Signal-to-Noise Ratio (PSNR), Root Mean Squire Error (RMSE), Standard Deviation (SD), smoothness, entropy, Structural Similarity (SSIM), and execution time. The results show that the contrast enhancement improves the radiographic image quality, the Wiener filter achieves better enhancement results than other filters, the curvelet transform denoising gives better enhancement than wavelet denoising. The bicubic interpolation with resolution factor two is promising in terms of the quality assessment metrics.

Keywords: *Radiographic image, Filtering, Denoising, Interpolation, Wavelet, Curvelet*

1. Introduction

Gamma-Radiography Testing (GRT) is one of the important applications of radioisotopes in the industry. It is used in several industries to assess the weld quality by evaluating the radiographs of the welded components. It has been used to check welds in pipelines that carry natural gas or oil. There are several advantages of gamma radiography compared to the other technologies. It can be done thoroughly and non-invasively, more rapidly, and cheaply. GRT uses gamma radioisotopes to inspect materials defects in the welds, where, a special film is taped over the weld around the outside of the pipe. A machine called a pipe crawler carries a shielded radioactive source to the position of the weld. The radioactive source is remotely exposed to the pipe and a radiographic image of the weld is produced on the film. This film is later developed and examined for signs of flaws in the weld. The interpretation of the radiographic film can be done automatically or by a skilled operator. For automatic interpretation, firstly the image is digitized, and then an enhancement process is carried out. After that detection and classification processes are performed. Figure 1 shows the block diagram of the automatic interpretation system using GRT.

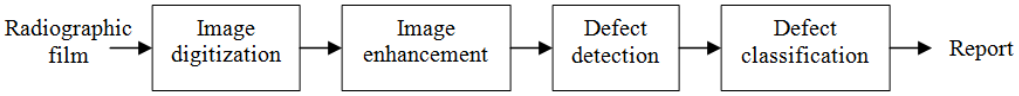

Figure 1. Block Diagram of the Automatic Interpretation System using GRT

The digitalization of radiographic films can be carried out using a digital camera or a digital scanner. After the digitization process, the produced images have small contrast between the background and the weld defect regions. Also some pronounced granularities are found due to digitization and the type of film used in industrial radiographic testing. So image enhancement is important in order to remove system noise and radiographic film noise. Radiographic image enhancement has been studied by several researchers using various techniques and approaches. Movafeghi et. al. used spatial and frequency (wavelet) domain techniques based on morphological transformations (Top-Hat and Bottom-Hat transforms) for enhancement of radiographic images [1]. Zhang et. al. proposed an enhancement algorithm for enhancement of radiographic images based on generalized fuzzy techniques. These algorithmic maps the image to the generalized fuzzy space through involving the concept of a generalized fuzzy set. Using the characteristics of generalized fuzzy transition with a large range, an image can satisfactory enhanced through processing the with a generalized fuzzy enhancement algorithm [2]. Wang et. al. used a median filter and wavelet thresholding for reducing the radiographic image noise, and used gamma correction and contrast limited adaptive histogram equalization to enhance the perception of defects. These processes are used to eliminate noise and background artifacts and to smooth sharp edges, in addition to the removal of some details in small objects [3]. Arulmozhi et. al. used a wavelet technique for denoising radiographic images and to find out the best filter that furnishes the maximum details of the radiographic image. The denoising operation is performed using a non orthogonal log-gabor wavelet function [4]. Frosio et. al. presented an algorithm for maximizing the contrast of a digital radiography automatically using an adequate gray level transform, whose parameters are computed on the basis of the image entropy and through maximization of the contrast enhancement effect [5].

The image quality evaluation remains a challenging task in radiological research. The objectives of this paper are performing some image processing techniques for radiographic image enhancement, and performing qualitative and quantitative evaluation of these techniques. This paper is organnized as follw; Section 2 presents the quality assessment metrics that will be used in the quantitative evaluation. Section 3 presents the contrast enhancement of the radiographic image. Section 4 presents the radiographic image filtering. Section 5 presents the denoising of the radiographic image. Section 6 presents the performed radiographic image interpolation methods. Finally, Section 7 gives the conclusion remarks.

2. Quality Assessment Metrics

For quantitative evaluation of the image enhancement processes, some parameters can be calculated for the enhanced image. These parameters are the MSE, PSNR, SSIM, entropy, SD, smoothness, and the execution time. The MSE is the arithmetic difference between the original image and the enhanced image and it measures the loss of image quality [6]. Consider the original image F (i, j) and the enhanced image G (i, j) with size M × N, the MSE can be defined as [7]:

$$MSE(F,G) = \frac{1}{MN}\sum_{i=0}^{M-1}\sum_{j=0}^{N-1}[F(i,j) - G(i,j)]^2 \quad (1)$$

The PSNR is the ratio between the maximum possible power of the image and the power of corrupting noise that affects the fidelity of its representation. PSNR is expressed in terms of a logarithmic decibel scale, and it is defined for an 8 bit level image as [7]:

$$PSNR(F,G) = 10 * \log_{10}\left(\frac{255^2}{MSE(F,G)}\right) \quad (2)$$

Logically, the lower value of the MSE means lower error, and hence the higher value of the PSNR is better. Here, the signal is the original image, and the noise is the error in reconstruction. The SSIM measures the image quality by capturing the similarity of images [8]. The similarities are measured in luminance, contrast, and structure. The luminance comparison function between the image F and the enhanced image G is defined as:

$$L(F,G) = \frac{2\mu_f\mu_g + s_1}{\mu_f^2 + \mu_g^2 + s_1} \quad (3)$$

where μ_f and μ_g are the mean values of F and G, respectively, and s_1 is a stabilizing constant, and it is included to avoid instability when μ_f and μ_g is very close to zero. It is defined as:

$$s_1 = (K_1 L)^2 \quad (4)$$

where L is the dynamic range of the pixel values (255 for 8-bit gray-scale images), and K_1 is a small constant less than 1. The contrast comparison function is defined as:

$$C(F,G) = \frac{2\sigma_f\sigma_g + s_2}{\sigma_f^2 + \sigma_g^2 + s_2} \quad (5)$$

where σ_f and σ_g are the standard deviations of F and G , respectively, and s_2 is a stabilizing constant. The structure comparison function is defined as:

$$S_c(F,G) = \frac{\sigma_{fg} + s_3}{\sigma_f\sigma_g + s_3} \quad (6)$$

where σ_{fg} is the correlation coefficient between and F and G and s_3 is a stabilizing constant. The SSIM is obtained by combining the three comparison functions [6, 8]:

$$SSIM(F,G) = [L(F,G)] \,.\, [C(F,G)] \,.\, S_c[(F,G)] \quad (7)$$

For $s_2=2s_3$,

$$SSIM(F,G) = \frac{2(2\mu_f\mu_g + s_1)(\sigma_{fg} + s_3)}{(\mu_f^2 + \mu_g^2 + s_1)(\sigma_f^2 + \sigma_g^2 + 2s_3)} \quad (8)$$

The entropy is a measure of the average information content. If P denotes the probability mass function of F, the entropy is defined by [9]:

$$E = -\sum_{i=1}^{n} P(F_i)\log_2 P(F_i) \tag{9}$$

The standard deviation (σ) is a measure of the dispersion of a set of data from its mean. The smoothness measures the relative smoothness of the intensity in an image region as follows [10]:

$$S = 1 - \frac{1}{1+\sigma^2} \tag{10}$$

3. Contrast Enhancement

Histogram equalization is an image enhancement technique, which improves the visual appearance of the image by assigning equal number of pixels to all available intensity values [11]. Image contrast can be maximized using adaptive histogram equalization by adaptively enhancing the contrast of each pixel relative to its local neighborhood. This process produces an improved contrast in the original image [12]. In this process, the histograms are calculated for small regional areas of pixels to produce local histograms, and then these local histograms are equalized or remapped from the often narrow range of intensity values to a wider range. Adaptive histogram equalization can provide better contrast in local areas than that can be achieved using traditional histogram equalization methods. The traditional methods process the entire image at once, where adaptive histogram equalization utilizes local contextual regions. Consider an image of size M × N, and a cumulative histogram H(g). The transfer function $F_{HE}(g)$ that maps the original gray levels into the transformed ones is defined as [13]:

$$F_{HE}(g) = G_{y\min} - (G_{y\max} - G_{y\min})\frac{H(g)}{MN} \tag{11}$$

where G_{ymax} and G_{ymin} are the upper and lower limits of the transformed gray levels, respectively. The adaptive histogram equalization is made adaptively by taking the histogram over a local region instead of the whole image as [14]:

$$F_{AHE}(g) = G_{y\min} + (G_{y\max} - G_{y\min})\frac{H_{AHE}(g)}{(MN)_{AHE}} \tag{12}$$

where $H_{AHE}(g)$ refers to the adaptive cumulative histogram. Figure (2.a) shows a digitized radiographic image, while figure (2.b) shows the enhanced image after adaptive histogram equalization.

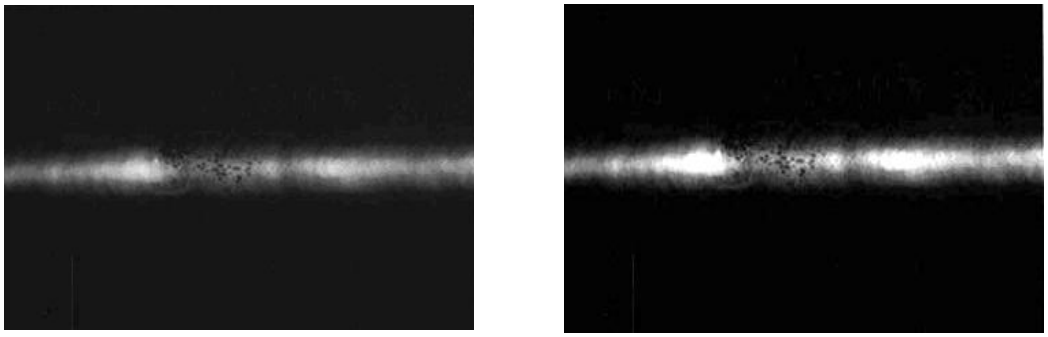

(a) Original radiographic image (b) Enhanced image using AHE

Figure 2. Adaptive Histogram Equalization Effect on Contrast Enhancement of the Radiographic Image

The above results show that the contrast enhancement improves the radiographic image quality.

4. Radiographic Image Filtering

Image filtering can be used to remove noise, sharpen contrast, or highlight contours in the radiographic images. Median and Wiener filters have been used in many previous researches [3, 13-16]. In this section, radiographic image filtering is carried out after contrast enhancement using median, Wiener, Lee, and Kuan filters in order to select the best filter for the radiographic image filtering purpose.

4.1 Median Filter

The median filter is a nonlinear filter used to remove noise from the image. It can potentially remove all the noise without affecting the clean pixels. It is the most frequently used filtering technique to remove impulsive noise from radiographic images. The median filter considers each pixel in the image and looks at its nearby neighbors, and then replaces the pixel value with the median of neighboring pixel values. The median is calculated by first sorting all the pixel values from the surrounding neighborhood, and then replacing the pixel being considered with the median value. Figures (3.b) and (3.c) show the effect of the median filters with 3×3 and 5×5 operating windows on the radiographic image.

4.2 Wiener Filter

The Wiener filter is designed by minimizing the MSE between the filtered image and the original image. It can be applied to the image, adaptively, tailoring itself to the local image variance. When the variance is large, it performs little smoothing. When the variance is small, it performs more smoothing. Since the intensities of the pixels in the weld area follow a Gaussian distribution. The Wiener filter was selected for filtering of radiographic images of welds, because it is close to the matched filter in this case [17]. Figure (3.d) shows the effect of the Wiener filter on the radiographic image.

4.3 Lee Filter

Lee filter uses the statistical distribution of the pixels in a moving window to estimate the value of the pixel of interest [18]. The Lee filter is based on the assumption that the mean and variance of the pixel of interest are equal to the local mean and variance of all pixels within the moving window. If the pixel value in the input image is x_i, μ_i is the mean value of the input image, and σ_i is the variance of the input image, then the output pixel value of the filtered image using Lee filter is defined as:

$$x_o = \mu_i + K(x_i - \mu_i) \tag{13}$$

where K is a weighting factor ranging from 0 to 1 and defined as:

$$K = \frac{K_1}{\sigma_i^2 \mu_i^2 + K_1}, \qquad K1 = \frac{\sigma_w + \mu_w^2}{\sigma_i^2 + 1} - \mu_w^2 \tag{14}$$

where μ_w and σ_w are the mean and variance of the pixels in the moving window, respectively. Figure (3.e) shows the effect of the Lee filter on the radiographic image.

4.4 Kuan Filter

Kuan filter [19] smoothes the image data, without removing edges or sharp features in the image. Firstly, it transforms the multiplicative noise model into a signal-dependent additive noise model. Then, the minimum MSE criterion is applied to the model. The resulting filter has the same form as the Lee filter but with a different weighting function. Because Kuan filter makes no approximation to the original model, it is superior to the Lee filter [20]. The Kuan filter has the same form as the Lee filter but with a different weighting factor K_1 defined as:

$$K_1 = \frac{\sigma_w + \mu_w^2}{\sigma_i^2 + 1 + \mu_i \sigma_i} - \mu_w^2 \tag{15}$$

Figure (3.f) shows the effect of the Kuan filter on the radiographic image. For quantitative evaluation of the image enhancement, the metrics discussed in Section 2 have been calculated for the filtered image and tabulated in Table (1).

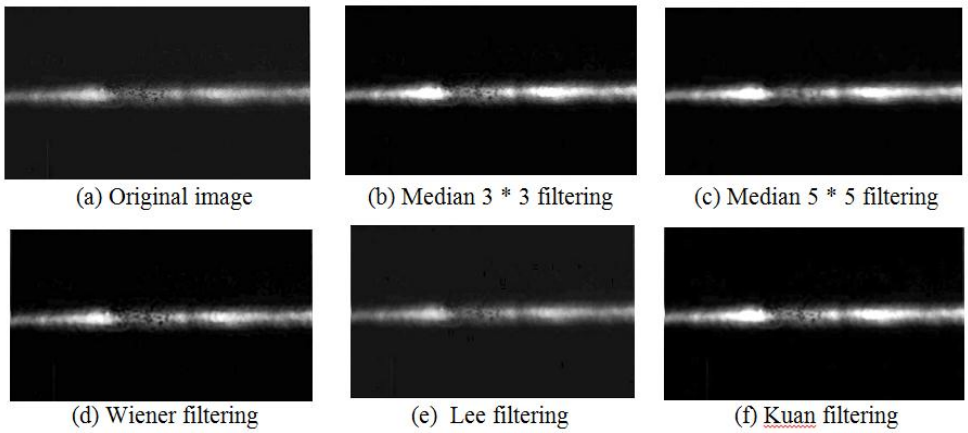

Figure 3. Radiographic Image Filtering

Table 1. Quantitative Evaluation of Radiographic Image Filtering

Enhancement process	RMSE	PSNR	Entropy	SD	Smoothness	SSIM	Time (Sec)
Contrast Enhancement	0.0865	21.0637	3.4211	0.1851	0.0331	0.9989	0.19
Median filtering (3*3)	0.0873	21.1835	2.8154	0.1829	0.0324	0.9989	0.15
Median filtering (5*5)	0.0867	21.2347	2.8451	0.1814	0.0319	0.9990	0.13
Wiener Filtering	0.0847	22.5282	3.6836	0.1806	0.0316	0.9992	0.35
Lee Filtering	0.0817	21.7581	3.4229	0.1576	0.0240	0.9989	613.8
Kuan Filtering	0.0800	21.9423	3.6017	0.1665	0..0270	0.9991	681.2

The above results show that the Wiener filter gives the lowest RMSE as it is designed by minimizing the MSE. This leads to its highest PSNR. The values of the entropy, the standard deviation, the image smoothness, and the structural similarity have small differences between the different filters. Lee and Kuan filters take longer times than the other filters. So, the Wiener filter can be considered as the best filter for radiographic image enhancement.

5. Radiographic Image Denoising

In this section, the radiographic image denoising is carried out using the wavelet and the curvelet transforms.

5.1 Wavelet Denoising

The wavelet transform has been used for image denoising in several applications [21-24]. It is a mathematical operation used to divide a given image into different subbands of different scales to study each scale separtely. The Discrete Wavelet Transform (DWT) is fast, linear and invertible. Hence, wavelet reconstruction is possible. DWT chooses a subset of scales and positions to calculate. A sample version of the wavelet coefficients $W_F(a,\eta)$ can reconstruct the original signal in an efficient way if the family of scaled and shifted mother wavelets of the selected a and η constitute an orthonogonal and complete basis [25]. The DWT of a signal F is calculated by passing it through a series of filters. Firstly, the samples are passed through a low pass filter with impulse response G_L resulting in a convolution of the two:

$$G(n) = (F * G_L)(n) = \sum_{k=-\infty}^{\infty} F(k) G_L(n-k) \tag{16}$$

The signal is also decomposed simultaneously using a high-pass filter with impulse response G_H. The outputs give the detail coefficients from the high-pass filter and the approximation coefficients from the low-pass. It is important that the two filters are related to each other to allow a perfect recomstruction. However, half of the signal frequencies have

now been removed, half of the samples can be discarded according to Nyquist's rule. The filter outputs are then subsampled by 2 as follows:

$$G_{low}(n) = \sum_{k=0}^{L} F(k) G_L(2n - k) \tag{17}$$

$$G_{high}(n) = \sum_{k=-0}^{L} F(k) G_L(2n - k) \tag{18}$$

where L is the length of the filter

The 2-D DWT is essentially a 1-D analysis of a 2-D image. It is performed by analyzing the rows and columns of an image in a separable fashion [26]. The first step applies the analysis filters to the rows of an image. This produces two new images, where one image is an approximation of row coefficients and the other is a set of detail row coefficients. After that, analysis filters are applied to the columns of the image, to produce four different images called subbands. Rows and columns are analyzed with a high pass filter and a low pass filter. Each subband provides different information about the image. The wavelet transform is constituted with different levels. The maximum level to apply the wavelet transform depends on how many data points contained in a data set, since there is a down-sampling by 2 operations from one level to the next one. The number of decomposition levels of the wavelet transform affects the noise removal from the image. There are several kinds of wavelets such Haar, Daubechies, Symlet and Biorthogonal. The choice of the wavelet determines the final waveform shape.

There are two common methods for thresholding of the resulting wavelet coefficients; hard thresholding and soft thresholding. In the hard thresholding, the coefficients with absolute values below the threshold are set to zero. The soft thresholding goes one step further and decreases the magnitude of the remaining coefficients by the threshold value. Hard thresholding maintains the scale of the signal but introduces ringing and artifacts after reconstruction due to the discontinuity in the wavelet coefficients. Soft thresholding eliminates this discontinuity resulting in smoother signals but slightly decreases the magnitude of the reconstructed signal [27]. Radiographic images after contrast enhancment and filtering using Wiener filter have been denoised using four wavelet types; Haar, Daubechies 4, Symlet, and Biorthogonal wavelets with different decomposition levels (DL) and soft thresholding. The results are shown in figure 4, and the quantitative evaluation is shown in Table 2.

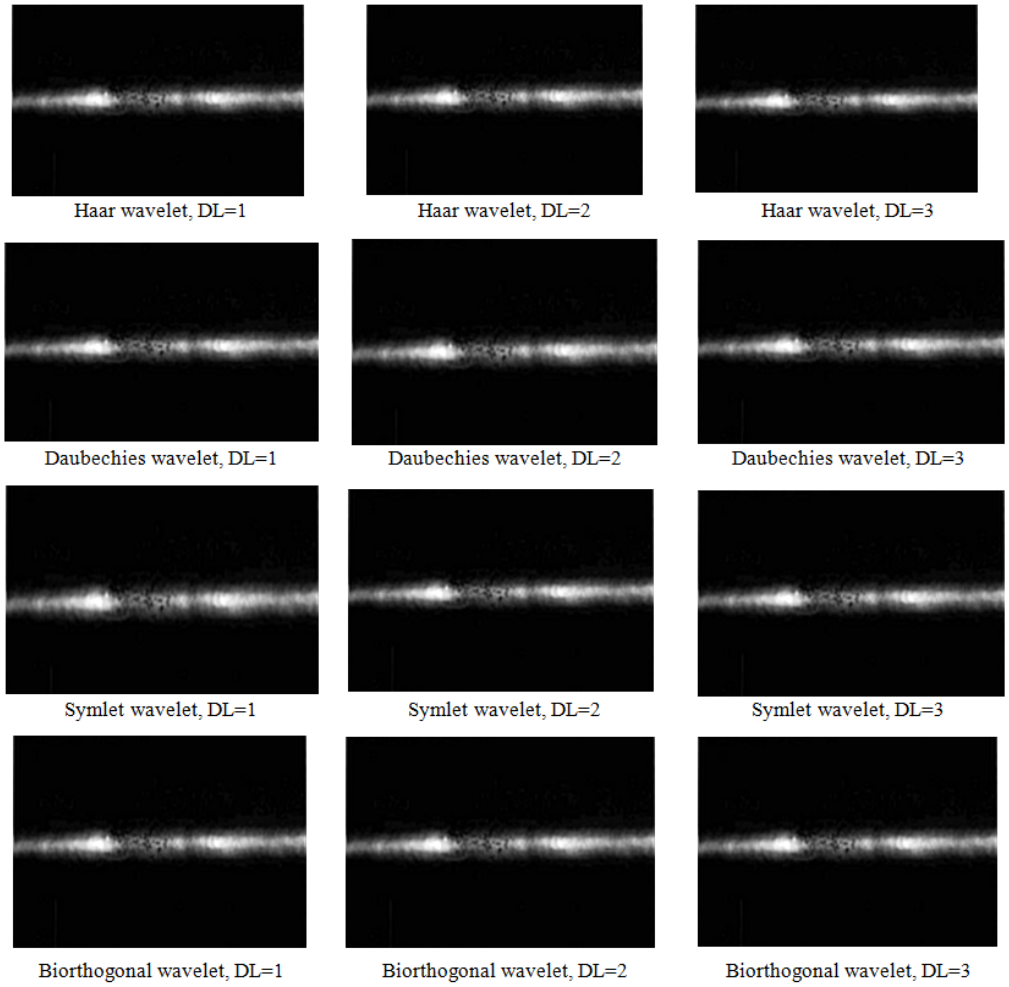

Figure 4. Image Denoising using Wavelet

5.2 Curvelet Denoising

The curvelet transform has been developed in the last few years to overcome inherent limitations of traditional multi-scale representations such as the wavelet transform [28]. One of the DWT disadvantages in image processing is that it gives a large number of coefficients in all scales corresponding to the edges of the image. This means that many coefficients are required in order to exactly reconstruct the edges in an image. This makes the DWT inefficient for handling long curved edges. Recent approaches like the ridgelet and curvelet transforms are more efficient in handling long linear and curvilinear singularities in an image [29, 30]. The curvelet transform is used to decompose the image into different subbands and partitioning is used to break each subband into tiles. Finally, the ridgelet transform is applied to each tile [31]. In this way, the image edges can be represented, efficiently by the ridgelet transform, because the image edges will now be almost like straight lines. Thus, the curvelet transform is an extension of the ridgelet transform to detect curved edges, effectively [32]. The curvelet transform can be obtained as the follows. The image is split up into four subbands Δ_1, Δ_2, Δ_3 and P_3, and tiling is performed on the subbands Δ_1, Δ_2, and Δ_3. The

discrete ridgelet transform is performed on each tile of the subbands Δ_1 and Δ_2, and Δ_3. The general curvelet reconstruction formula is given by [33]:

$$P = \sum_{l=1}^{n-1} \Delta_l + P_n \tag{19}$$

where the planes Δ_l contain high-frequency details and P_n is a low-frequency approximation component. The curvelet transform has been used for image denoising [34- 35]. The curvelet denoised image is shown in figure (5), and the quantitative evaluation is shown in Table (2).

Table 2. Quantitative Evaluation of Radiographic Image Denoising

DL	Wavelet	RMSE	PSNR	Entropy	SD	Smoothness	SSIM	Time (Sec)
1	Haar	0.0627	24.0480	4.4197	0.1485	0.9986	0.9967	3.2190
	Db4	0.0574	24.8252	4.4138	0.1485	0.9986	0.9934	4.4060
	Sym	0.0575	24.8064	4.4138	0.1485	0.9986	0.9945	5.7580
	Bior	0.0569	24.9142	4.4139	0.1485	0.9986	0.9956	5.6701
2	Haar	0.0459	26.7672	4.5827	0.1485	0.9986	0.9934	4.9071
	Db4	0.0539	25.3694	4.4139	0.1485	0.9986	0.9925	6.0011
	Sym	0.0542	25.3214	4.4139	0.1485	0.9986	0.9912	7.8712
	Bior	0.0584	24.6730	4.4140	0.1485	0.9986	0.9946	7.8901
3	Haar	0.0502	25.9874	4.4141	0.1485	0.9986	0.9954	6.7810
	Db4	0.0584	24.6681	4.4136	0.1485	0.9986	0.9922	7.5672
	Sym	0.0584	24.6727	4.4139	0.1485	0.9986	0.9915	7.6623
	Bior	0.0570	24.8791	4.4055	0.1485	0.9986	0.9927	7.9814
Curvelet		0.0456	26.8152	4.6038	0.1485	0.9986	0.9939	5.4560

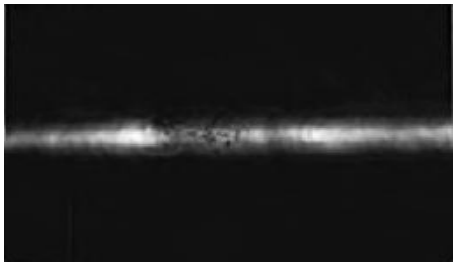

Figure 5. Image Denoising using Curvelet

The above results show that the standard deviation and the image smoothness are constant for all wavelet types at different decomposition levels. The Haar wavelet transform gives the highest PSNR, highest SSIM and the lowest RMSE values. By increasing the decomposition level, the PSNR is decreased and the processing time is increased. So, using the Haar wavelet with decomposition level 2 is the best for wavelet denoising. Curvelet denoising provides a little improvement in the PSNR compared to wavelet denoising.

6. Radiographic Image Interpolation

The image interpolation process aims to estimate intermediate pixels between the known pixel values by guessing the intensity values at missing locations. In 1-D interpolation, it is performed row-by-row and then column-by-column. If we have a discrete sequence $f(x_k)$ of length N and this sequence is filtered and down-sampled by 2, then we get another sequence $g(x_n)$ of length N/2. The interpolation process aims to estimate a sequence $l(x_k)$ of length N, which is as close as possible to the original discrete sequence $f(x_k)$. For equally spaced 1-D sampled data $g(x_n)$, several interpolation functions can be used. The value of the sample to be estimated $l(x_{k+1})$ can be written in the form [31]:

$$l(x_{k+1}) = \sum_{n=-\infty}^{\infty} c_n \beta(x_{k+1} - x_n) \tag{20}$$

where $\beta(x)$ is the interpolation basis function. From the classical sampling theory [32], if $g(x_n)$ is band-limited to $[-\pi,\pi]$ then:

$$l(x_{k+1}) = \sum_{n=-\infty}^{\infty} g(x_n)\,\mathrm{sinc}(x_{k+1} - x_n) \tag{21}$$

This is known as ideal interpolation, but it is not practical due to the slow rate of decay of the interpolation kernel. So, approximations such as the bilinear, bicubic and cubic spline interpolation formulas are used as alternatives [32,33]. If the distance between x_{k+1} and x_n is s, then the distance between x_{k+1} and x_{n+1} is 1-s, the value of $l(x_{k+1})$ can be written in the form [33]:

$$l(x_{k+1}) = (1-s)g(x_n) + sg(x_{n+1}) \tag{22}$$

Bicubic interpolation produces noticeably sharper images than the previous two methods, and may achieve the ideal combination of processing time and output quality. The value of $l(x_{k+1})$ in bicubic interpolation is written as [33]:

$$\begin{aligned} l(x_{k+1}) = {} & g(x_{n-1})(-s^3 + 2s^2 - s)/2 + g(x_n)(3s^3 - 5s^2 + 2)/2 \\ & + g(x_{n+1})(-s^3 + 4s^2 + s)/2 + g(x_{n+2})(s^3 - s^2)/2 \end{aligned} \tag{23}$$

In cubic spline interpolation, the value of $l(x_{k+1})$ is written as [36-38]:

$$\begin{aligned} l(x_{k+1}) = {} & g(x_{n-1})[(3+s)^3 - 4(2+s)^3 + 6(1+s)^3 - 4s^3]/6 + g(x_n)[(2+s)^3 \\ & - 4(1+s)^3 + 6s^3]/6 + g(x_{n+1})[(1+s)^3 - 4s^3]/6 + g(x_{n+2})s^3/6 \end{aligned} \tag{24}$$

Figure (6) shows the results of the three interpolation methods with different resolutions, and Table (3) shows the quantitative evaluations of images enhancement using interpolation. The Resolution Factor (RF) represents the ratio between the resolution of the interpolated image and the resolution of the available image.

Table 3. Quantitative Evaluations of Images Enhancement using Image Interpolation

Interpolation method	Resolution factor	Entropy	SD	Smoothness	Time (Sec)
Bilinear	2	6.6054	0.1479	0.0214	1.21
	5	6.6122	0.1479	0.0214	2.40
	10	6.9038	0.1479	0.0214	7.57
Bicubic	2	6.9038	0.1479	0.0214	2.39
	5	6.9052	0.1479	0.0214	4.45
	10	6.9053	0.1479	0.0214	11.75
Spline	2	6.8744	0.1479	0.0214	3.06
	5	6.8712	0.1479	0.0214	5.56
	10	6.8991	0.1479	0.0214	14.71

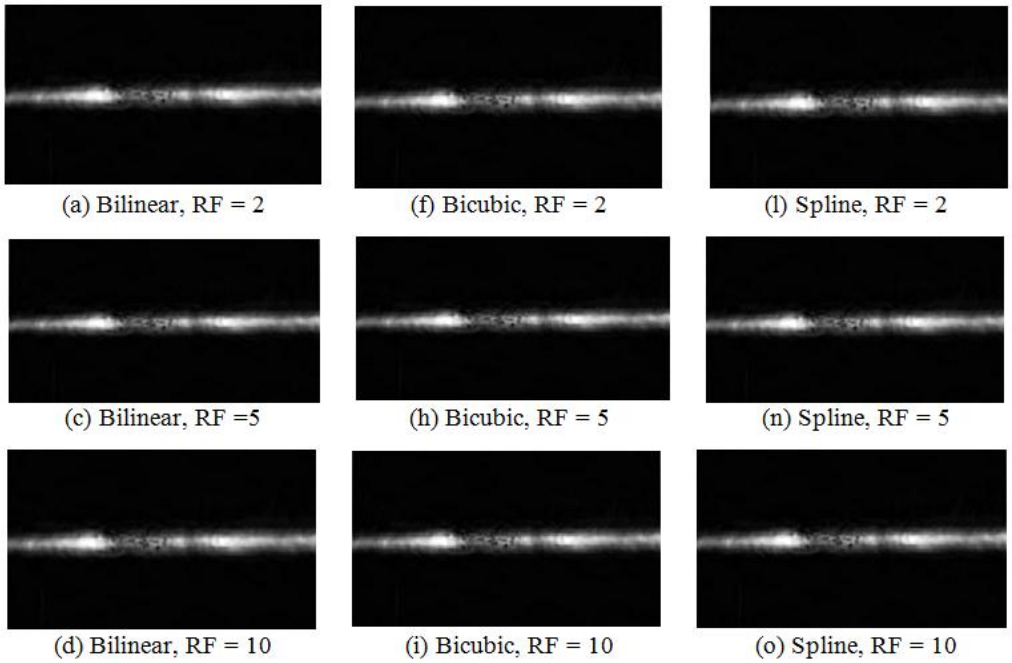

Figures (6) Radiographic image interpolation

The above results show that the bicubic interpolation gives the highest entropy, while the standard deviation and the image smoothness are not affected by the interpolation method or by the resolution factor. Increasing the resolution increases the entropy, but at the expense of time. So, bicubic interpolation with RF=2 can be considered suitable for radiographic image interpolation.

7. Conclusions

The paper presented some image processing techniques for radiographic image enhancement. The results have been evaluated qualitatively and quantitatively considering the PSNR, RMSE, standard deviation, smoothness, entropy, structural similarity, and execution

time. The radiographic image enhancement techniques discussed in the paper can constitute a solid basis for efficient weld defect detection applications from radiographic images.

References

[1] A. Movafeghi, M. Taheri, M. H. Kargarnovin, F. Ghasemi, B. Rokrok, M.Seiedi, K. Edaalati, A. Kermani and N. Rastkhah, "Quality Improvement of Digitized Radiographs by Filtering Technique Development Based on Morphological Transformations", Nuclear Science Symposium Conference, vol. 3, **(2004)**, pp. 1845 – 1849, Rome.

[2] Z. Xiao-guang, G. Ding and X. Jian-jian, "Generalized Fuzzy Enhancement of Image for Radiographic Testing Weld", 4th International Symposium on Image and Signal Processing and Analysis, **(2005)**, pp. 94-99.

[3] X. Wang, B. S. Wong, C. G. Tui, K. P. Khoo and F. Foo, "Image Enhancement for Radiographic Non-Destructive Inspection of The Aircraft", Asia-Pacific Conference on NDT, New Zealand, **(2006)**.

[4] N. Arulmozhi, N. Manoharan, R. B. Sheela, B. Venkatraman and R. Baldev, "Isolation of Defects in Radiographic Weld Images With Wavelet Denoising Using Log-Gabor Filter", International Conference on Computational Intelligence and Multimedia Applications, **(2007)**, pp. 394-399.

[5] I. Frosio, M. Lucchese, F. Lissandrello and N. A. Borghese, "Automatic Contrast Enhancement in Digital Radiography", Nuclear Science Symposium Conference Record, **(2008)**, pp. 4331 – 4334.

[6] H. R. Sheikh and A. C. Bovik, "Image Information and Visual Quality", Transactions on Image Processing, vol. 15, no. 2, **(2006)**, pp. 430 – 444.

[7] C. Yim and A. C. Bovik, "Quality Assessment of Deblocked Images", IEEE Transactions on Image Processing, vol. 20, no. 1, **(2011)**, pp. 88-98.

[8] Z. Wang, A. C. Bovik, H. R. Sheikh and E. P. Simoncelli, "Image Quality Assessment: From Error Visibility to Structural Similarity", IEEE Transactions on Image Processing, vol. 13, no. 4, **(2004)**, pp. 1-14.

[9] T. R. Wojcik and D. Krapf, "Solid-State Nanopore Recognition and Measurement Using Shannon Entropy", IEEE Photonics Journal, vol. 3, no. 3, **(2011)**, pp. 337-343.

[10] F. G. Hashad, T. M. Halim S. M. Diab, B. M. Sallam and F. E. Abd El-Samie, "A Hybrid Algorithm for Fingerprint Enhancement", International Conference on Computer Engineering & Systems, **(2009)**, pp. 57 – 62, Cairo, Egypt.

[11] D. Coltuc, P. Bolon and J. M. Chassery, "Exact Histogram Specification", IEEE Transactions on Image Processing, vol. 15, no. 5, **(2006)**, pp.1143-1152.

[12] E. D. Pisano, E. B. Cole, B. M. Hemminger, M. J. Yaffe, S. R. Aylward, A. D. A. Maidment, R. E. Johnston, M. B. Williams, L.T. Niklason, E. F. Conant, L. L. Fajardo, D. B. Kopans, M.E. Brown and S. M. Pizer, "Image Processing Algorithms for Digital Mammography: A Pictorial Essay", Radiographics, vol. 20, **(2000)**, pp. 1479-1491.

[13] S. M. Alghalandis and G. H. Nozad, "Welding Defect Pattern Recognition in Radiographic Images of Gas Pipelines Using Adaptive Feature Extraction Method and Neural Network Classifier", 23rd World Gas Conference, Amsterdam, **(2006)**.

[14] X. Wanga and B. S. Wong, "Image Enhancement for Radiography Inspection", NDT.net, vol. 10, no.4, **(2005)**.

[15] I. Frosio and N. A. Borghese, "Statistical Based Impulsive Noise Removal in Digital Radiography" , IEEE Transactions on Medical Imaging, vol. 28, no. 1, **(2009)**, pp. 3-16.

[16] T. W. Liao, D. M. Li and Y. M. Li, "Extraction of Welds from Radiographic Images Using Fuzzy Classifiers", Informatics and Computer Science: An International Journal, vol. 126, **(2000)**, pp. 21–42.

[17] G. Wang and T. W. Liao, "Automatic Identification of Different Types of Welding Defects in Radiographic Images", NDT & E International, vol. 35, **(2002)**, pp. 519-528.

[18] S. Lee, "Speckle Analysis and Smoothing of Synthetic Aperture Radar Images", Computer Graphics Image processing, vol.17, **(1981)**, pp. 24-32.

[19] D. T. Kuan, A. A. Sawchuk, T. C. Strand and P. Chavel, "Adaptive Restoration of Images With Speckle", IEEE Transactions on Acoustics Speech Signal Processing, vol. ASSP-35, **(1987)**, pp.373-383.

[20] K. Arulmozhi, S. A. Perumal, K. Kannan and S. Bharathi, "Contrast Improvement of Radiographic Images in Spatial Domain by Edge Preserving Filters", International Journal of Computer Science and Network Security, vol.10, no.2, **(2010)**, pp. 233-240.

[21] S. G. Chang, B. Yu and M. Vetterli, "Adaptive Wavelet Thresholding for Image Denoising and Compression", IEEE Transactions on Image Processing, vol. 9, no. 9, **(2000)**, pp.1532-1546,.

[22] J. Portilla, V. Strela, M. J. Wainwright and E. P. Simoncelli, "Image Denoising Using Scale Mixtures of Gaussians in The Wavelet Domain", IEEE Transactions on Image Processing, vol. 12, no. 11, **(2003)**, pp. 1338-1351.

[23] F. Luisier, T. Blu and M. Unser, "Image Denoising in Mixed Poisson–Gaussian Noise", IEEE Transactions on Image Processing, vol. 20, no. 3, **(2011)**, pp.696-708.
[24] S. K. Mohideen, S. A. Perumal and M. M. Sathik, "Image De-noising Using Discrete Wavelet Transform", International Journal of Computer Science and Network Security, vol. 8, no. 1, **(2008)**, pp. 213-216.
[25] F. Bömers, "Wavelets in Real Time Digital Audio Processing: Analysis and Sample Implementations", M. Sc. Thesis, Department of Computer Science, University of Mannheim, **(2000)**.
[26] D. L. Ward, "Redundant discrete wavelet transform based super-resolution using sub-pixel image registration", M. Sc. Thesis, Department of the Air Force, Air University, **(2003)**.
[27] B. C. Rao and M. M. Latha, "Selective Neighbouring Wavelet Coefficients Approach For Image Denoising", International Journal of Computer Science and Communication, vol. 2, no. 1, **(2011)**, pp. 73– 77.
[28] E. J. Candes and D. L. Donoho, "New Tight Frames of Curvelets and Optimal Representations of Objects With Piecewise C^2 Singularities", Communications on Pure and Applied Mathematics, vol. 57, no. 2, **(2004)**, pp. 219–266.
[29] F. E. Ali, I. M. El-Dokany, A. A. Saad and F. E. Abd El-Samie, "Curvelet Fusion of MR and CT images," Progress In Electromagnetics Research C, vol. 3, **(2008)**, pp. 215-224.
[30] J. L. Starck, P. Abrial, Y. Moudden and M. K. Nguyen, "Wavelets, Ridgelets and Curvelets on the Sphere", Astronomy and Astrophysics, vol. 446, **(2006)**, pp.1191-1204.
[31] F. E. Ali, "Processing of Magnetic Resonance Images", M. Sc. Thesis, Faculty of Electronic Engineering, Menofia University, **(2009)**.
[32] F. E. Ali, I. M. El-Dokany, A. A. Saad and F. E. Abd El-Samie, "A Curvelet Transform Approach for The Fusion of MR and CT Images", Journal of Modern Optics, vol. 57, no. 4, **(2010)**, pp.273 – 286.
[33] J. L. Starck, E. Candes and D. L. Donoho, "The Curvelet Transform for Image Denoising", IEEE Transactions on Image Processing, vol. 11, no. 6, **(2002)**, pp. 670 -684.
[34] R. Sivakumar, "Denoising of Computer Tomography Images Using Curvelet Transform", ARPN Journal of Engineering and Applied Sciences, vol. 2, no. 1, **(2007)**.
[35] A. D. Ali, P. D. Swami and J. Singhai, "Modified Curvelet Thresholding Algorithm for Image Denoising", Journal of Computer Science, vol. 6, no. 1, **(2010)**, pp. 18-23.
[36] M. Unser, A. Aldroubi and M. Eden "B-Spline Signal Processing: Part I- Theory", IEEE Transactions on Signal Processing, vol. 41, no.2, **(1993)**, pp. 821-833.
[37] G. Ramponi, "Warped Distance for Space Variant Linear Image Interpolation", IEEE Transactions on Image Processing, vol. 8, **(1999)**, pp. 629- 639.
[38] P. Thevenaz, T. Blu and M. Unser, "Interpolation Revisited", IEEE Transactions on Medical Imaging, vol. 19, no.7, **(2000)**, pp. 739-758.

Authors

Hani Kasban received the B. Sc., M. Sc. And Ph. D. degrees in Electrical Engineering from Menoufia University, Egypt in 2002, 2008 and 2012, respectively. He is currently an Assistant Lecturer in the Department of Engineering and Scientific Instruments., Nuclear Research Center (NRC), Egyptian Atomic Energy Authority (EAEA), Cairo, Egypt. He is a co-author of many papers in national and international conference proceedings and journals. He is currently working towards the Ph.D. degree in Electronic Engineering from the Menoufia University. His current research areas of interest include radiation applications, image processing, and signal processing.

Osama Zahran received the B.Sc. (Honors), from the Faculty of Electronic Engineering, Menoufia University, Menouf, Egypt, in 1997, and the Ph. D. degree from The University of Liverpool in 2006. He joined the teaching staff of the Department of Electronics and Electrical Communications, Faculty of Electronic Engineering, Menoufia University, Menouf, Egypt. He is a co-author of about 29 papers in national and international conference proceedings and journals. His

current research areas of interest include Nano-scale devices, expert systems, artificial intelligence and hybrid intelligent systems.

Horya Arafa received the B.Sc. (Honors), M.Sc from the Faculty of Engineering, Cairo University, and PhD in Mechanical Engineering from the Faculty of Engineering, Zagazig University, Egypt. She joined the teaching staff of the Department of Engineering and Scientific Instruments., Nuclear Research Center (NRC), Egyptian Atomic Energy Authority (EAEA), Cairo, Egypt, in 1983. Currently, she is the Egyptian project co-coordinator of project RAF 8/040 "Radioisotope Applications for Troubleshooting and Optimizing Industrial Processes".

Mohamad Elkordy received the B.Sc. (Honors), M.Sc., and PhD. from the Faculty of Electronic Engineering, Menoufia University, Menouf, Egypt, in 1979, 1985, and 1991, respectively. He joined the teaching staff of the Department of Electronics and Electrical Communications, Faculty of Electronic Engineering, Menoufia University, Menouf, Egypt, in 1991. His current research areas of interest include SAW applications, radiation applications, image processing, and signal processing.

Sayed M. El Araby received the B.Sc. (Honors), M.Sc., and PhD from the Faculty of Engineering, Ain Shams University, Cairo, Egypt, in 1976, 1984, and 1993, respectively. He joined the teaching staff of the Department of Engineering and Scientific Instruments., Nuclear Research Center (NRC), Egyptian Atomic Energy Authority (EAEA), Cairo, Egypt, in 1993. His current research areas of interest include Artificial Intelligence, Instrumentation and Control.

Fathi E. Abd El-Samie received the B.Sc. (Honors), M.Sc., and PhD. from the Faculty of Electronic Engineering, Menoufia University, Menouf, Egypt, in 1998, 2001, and 2005, respectively. He joined the teaching staff of the Department of Electronics and Electrical Communications, Faculty of Electronic Engineering, Menoufia University, Menouf, Egypt, in 2005. He is a co-author of about 100 papers in national and international conference proceedings and journals. He has received the most cited paper award from Digital Signal Processing journal for 2008. His current research areas of interest include image enhancement, image restoration, image interpolation, superresolution reconstruction of images, data hiding, multimedia communications, medical image processing, optical signal processing, and digital communications.